Bulletin of the Seismological Society of America, Vol. 93, No. 5, pp. 2236–2252, October 2003

Generation of New Cracks Accompanied by the Dynamic Shear Rupture Propagation of the 2000 Tottori (Japan) Earthquake

by L. A. Dalguer, K. Irikura, and J. D. Riera

Abstract The 2000 Tottori (Japan) earthquake caused fracture zones of surface rupture at some places away from the trace of the main causative fault. In order to explain this observation, the 3D dynamic rupture process of the 2000 Tottori (Japan) earthquake was simulated. The attractive feature of the problem under consideration is the possibility of introducing internal new cracks that propagate under tensile stress as a consequence of the dynamic process of shear slip propagation. The discrete element method was used to solve this problem because it can introduce internal tensile cracks. For the shear rupture propagation the simple slip-weakening model was used as a friction law on the fault. The new tensile cracks occur, following the classical Griffith theory, when the critical value of tensile fracture surface energy has been reached. The first step to solve the problem was the estimation of the dynamic parameters, such as stress drop, strength excess, and critical slip, which were recovered from the results of waveform inversion. In the second step, a shear dynamic rupture process was simulated assuming that shear slip occurs only on the pre-existing fault, and the tensile stress concentration resulting from shear slip causes the new cracks that propagate away from the pre-existing fault. The results, which are consistent with the observations, show a free-surface rupture caused by the new cracks and the development of a flowerlike structure springing from the borders of the pre-existing fault and main asperity.

Introduction

The 2000 Tottori (Japan) earthquake (M_j 7.3) was originated on a fault plane with strike N150°E (Fig. 1) and a dip nearly vertical (86°). According to the fine aftershock distribution analyzed by Fukuyama *et al.*, (2001), the earthquake could be originated from multiple segments. During field observations reported by Fusejima *et al.* (2000) after the 2000 Tottori (Japan) earthquake, several cracks were found on the free surface parallel to the trace of the causative fault (Fig. 2). Ueta *et al.* (2002) reported fracture zones in an existing tunnel 200 m below the surface in the epicentral area. The seismic profiling from a reflection survey done in the 2000 Tottori (Japan) earthquake area and analyzed by Inoue *et al.* (2001) suggests the existence of fractures developed as a flower structure near the free surface (Fig. 3). In order to get a better understanding of the surface rupture and possible flower structure caused by this earthquake, a full dynamic rupture process analysis involving the three basic modes of rupture (modes I, II, and III) is required. Dalguer *et al.* (2003) solved numerically this kind of problem for a pure strike-shallow fault embedded in a 3D elastic medium. They showed that the generation of tensile cracks (mode I) during shear slipping (modes II and III) could form a flowerlike structure and some of these cracks could reach the free surface. This idea looks plausible as a basis of analysis of the cracks generated during the 2000 Tottori (Japan) earthquake. Furthermore, the possibility of the occurrence of tensile cracks during the dynamic simulation of an earthquake is supported by laboratory observations, which suggest that a large number of tensile microcracks are generated during shear slipping (e.g., Cox and Scholz, 1988; Petit and Barquins, 1988; Anders and Wiltschko, 1994; Moore and Lockner, 1995), and also by the numerical and field investigation of brittle faults carried out by Vermilye and Scholz (1998). They showed that the tensile microcrack zone occurs within a volume of rock surrounding the fault tip. Such a zone may form before, during, or after growth of the shear plane.

The cracks generated during the Tottori earthquake were simulated using the model proposed by Dalguer *et al.* (2003). For the numerical simulation of the dynamic rupture process of the Tottori earthquake involving the three basic modes (mode I, II and III), we assumed a pre-existing fault for development of shear cracks, and tensile stress concentrations resulting from slip on this fault cause mode I cracks that propagate away from the fault. For shear rupture propagation, a simple slip-weakening model was used as the fric-

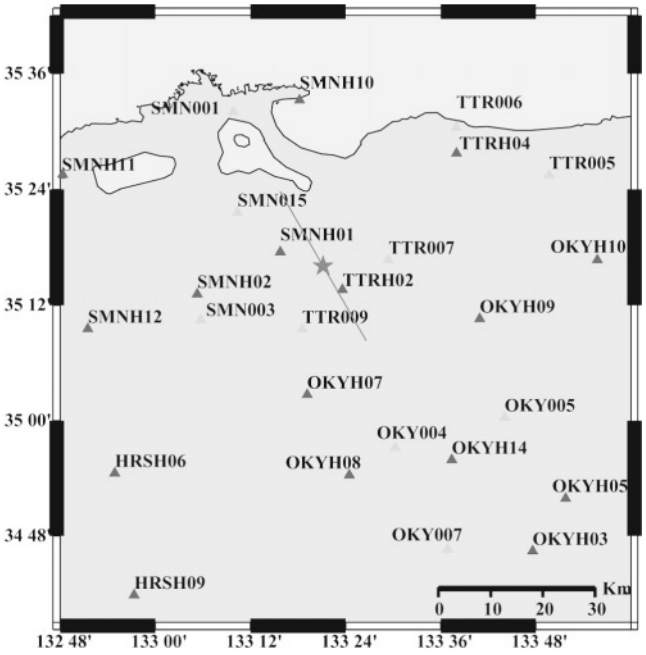

Figure 1. Map of the Tottori area. The straight line is the location of the fault model of the 2000 Tottori earthquake used for the simulation, and the black and gray triangles are, respectively, the stations records of Kiknet and Knet used for comparison.

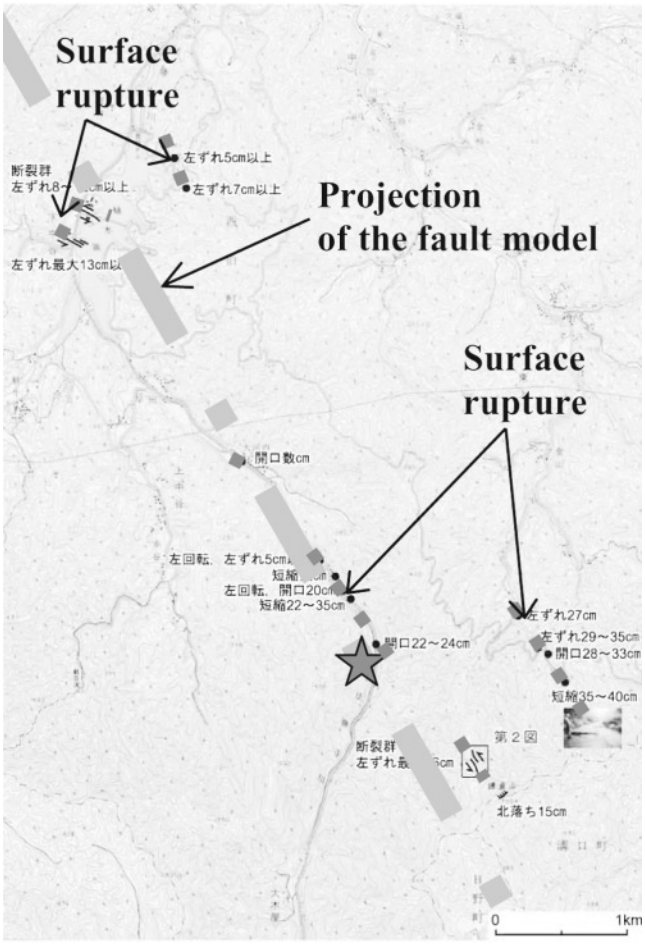

Figure 2. Surface rupture near the epicenter area of the 2000 Tottori earthquake (after the field observation developed by Fusejima *et al.* [2001].)

tion law on the pre-existing fault. For new tensile cracks, however, fracture follows the classical linear elastic fracture mechanics (LEFM) theory (Griffith, 1920) when the critical value of tensile fracture surface energy is reached. For this purpose the discrete element method (DEM) was used because it allows the generation of new tensile cracks with little difficulty.

Description of the Numerical Solution and Constitutive Relations

The DEM used in the analysis models any orthotropic elastic solid. The model consists of a 3D periodic trusslike structure that has cubic elements (Fig. 4). Nayfeh and Hefzi (1978) established the equivalence requirements between the cubic arrangement and an orthotropic elastic medium. Detailed descriptions of the DEM formulation can be found in Dalguer (2000) and Dalguer *et al.* (2001b). The method was used successfully with a simplified 2D model to simulate the dynamic shear rupture process of the 1999 Chi-Chi (Taiwan) earthquake (Dalguer *et al.*, 2001a,b). For 3D problems, Dalguer *et al.* (2002) calculated the dynamic and static shear stress changes during the rupture process of the 2000 Tottori earthquake, and Dalguer *et al.* (2003) simulated tensile crack generation by 3D dynamic shear rupture. The advantage of the DEM is the ease of introducing internal tensile cracks with little computational effort and without increasing the number of degrees of freedom of the system.

The solids of the DEM are represented as an array of normal and diagonal bars linking lumped nodal masses (Fig. 4a,b). The uniaxial elastic forces, Fe, acting along the bars, are given by

$$Fe_j = AE_j\varepsilon_j, \tag{1}$$

where ε_j is the axial deformation of bar j, and AE_j is the cross-sectional axial stiffness of the bar j. The calculation of the equivalent values of AE_j was discussed by Dalguer *et al.* (2001b). The representation of the elastic forces in the form given by equation (1) is very convenient for simulating tensile cracks, as explained later. Dynamic analysis was performed by means of an explicit numerical integration in the time domain. At each step of integration the nodal equilibrium, represented by equation (2), is solved by the central finite differences scheme. This scheme is a second-order accurate approximation of the first derivative.

$$m\ddot{u}_i + c\dot{u}_i = f_i, \tag{2}$$

where m denotes the nodal mass, c is the damping constant,

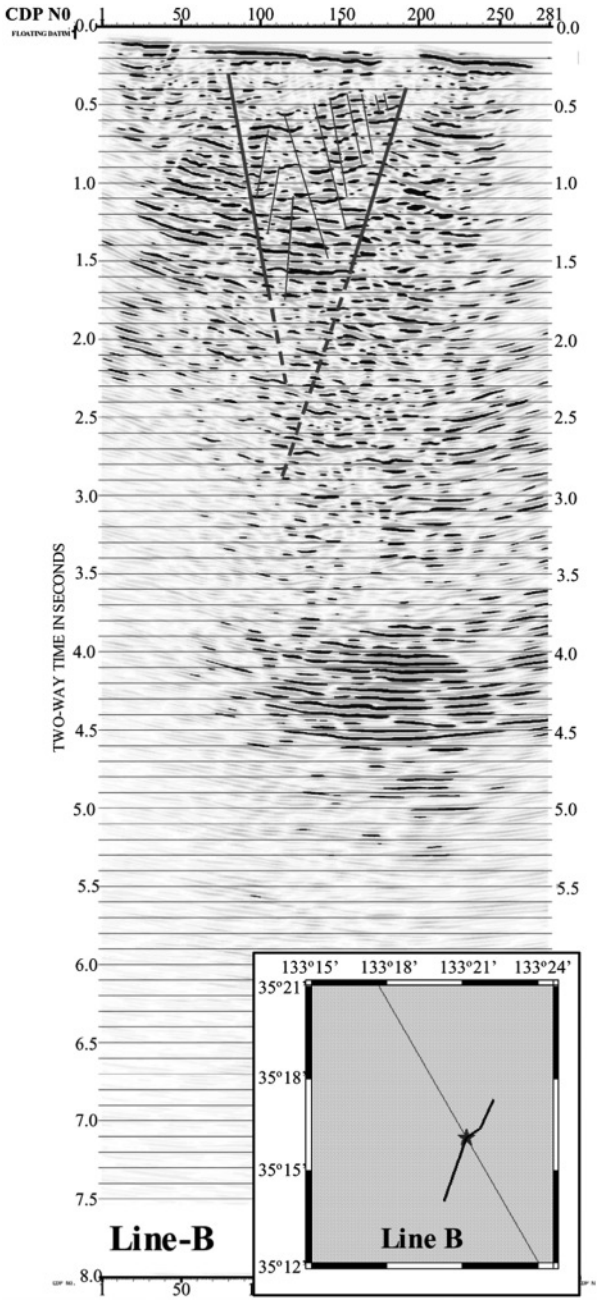

Figure 3. Seismic profile until 5–6 km depth corresponding to line B developed by Inoue *et al.* (2001). The straight lines show discontinuities like a flower structure in approximately 2.0 km depth. At the bottom of the figure is the location of line B. The straight line is the projection of the fault model for the simulation of the 2000 Tottori earthquake. The star is the epicenter.

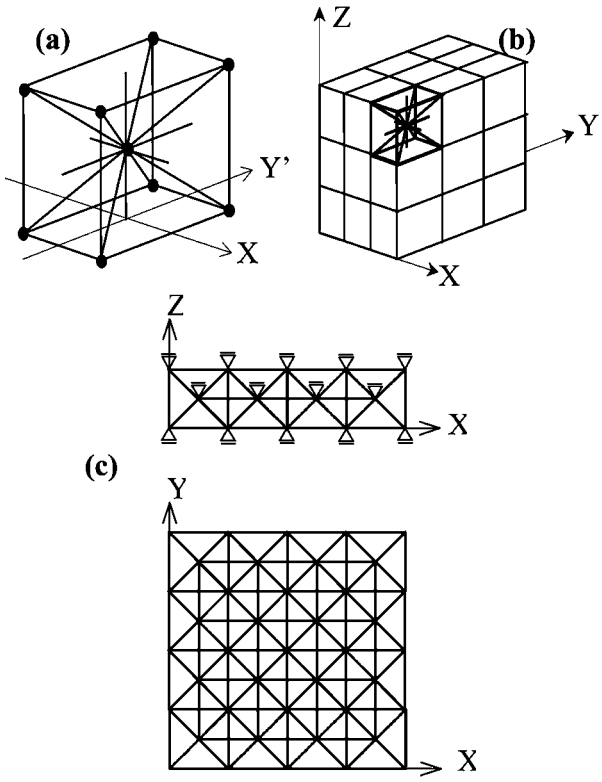

Figure 4. Numerical model used for the dynamic simulation (DEM): (a) basic cubic module, (b) generation of prismatic body for 3D model, and (c) representation of a plane strain state (no z displacements) for 2D model.

$\dot{u}_i$ and $\ddot{u}_i$ respectively are components of the velocity and acceleration vectors, and f_i is a component of the resultant forces at one nodal point that include elastic, external, and frictional forces in the i direction of the motion. In the current model, only those nodal points that coincide with the pre-existing fault (once it breaks) are under frictional force governed by any predefined friction law. The damping constant, c, was assumed to be proportional to the rigidity, k, of the bars of each cubic element; that is, $c = d_f k$, where d_f was assumed to be 0.005. For this value, the critical damping ratio (ξ) is approximately less than or equal to 0.045, corresponding to the first fundamental frequency (around 2.9 Hz) of one nodal point of the DEM. This formulation tries to represent the internal damping of the system, which is in general difficult to define, especially in lowly damped systems. In addition to this internal damping, this formulation contains an artificial damping needed in order to eliminate spurious high-frequency vibrations. Then, the choice of the damping in our formulation is a numerical problem. At any rate, damping was chosen after many numerical experiments in order to obtain stable results of slip velocity and waveform.

As stated, shear rupture propagates only along a weakness zone and involves sliding with friction. In our model, this zone was defined as a pre-existing fault, in which only shear slip, governed by a friction law, takes place. We adopted the simple slip-weakening friction model in the form given by Andrews (1976). This friction law, first proposed by Ida (1972), is used extensively for dynamic simulation of fault rupture processes (e.g., Day, 1982; Olsen *et al.*, 1997; Fukuyama and Madariaga, 1998; Harris and Day,

1999; Dalguer *et al.*, 2001a,b). In addition to providing a plausible model for shear dynamic rupture propagation, its use is supported by experimental laboratory findings for sliding friction on rock (e.g., Ohnaka *et al.*, 1987).

The behavior of uniaxial tensile stress-strain in rock (e.g., Atkinson, 1987) shows strain softening after the peak stress is reached. Therefore, the constitutive model for pure mode I is stress versus crack-opening displacement obtained from the displacement-controlled direct tension test (Atkinson, 1987). A material behaving in this manner would show gradual damage zone development. This is related to the critical tensile fracture energy, G_{Ic}, of LEFM, which has its roots in Griffith's energy balance concept. Therefore, extension of a fracture occurs once G_{Ic} has been reached or exceeded.

The constitutive relationship for the tensile stress-strain adopted for each bar element of the DEM is shown in Figure 5a. The loading–unloading path of the stress on each bar is shown in Figure 5b. A similar model was used successfully by Riera and Rocha (1991) to solve dynamic tensile crack propagation in 2D problems. The critical tensile stress, σ_{c}, can be derived from equation (1) or directly from Figure 5a:

$$\sigma_{\mathrm{c}} = E\varepsilon_{\mathrm{p}}, \tag{3}$$

where ε_{p} is the maximum elastic strain.

The critical fracture energy, G_{Ic}, for the DEM is the area of the inelastic zone of the stress-strain relationship shown in Figure 5a. Equation (3) gives

$$G_{\mathrm{Ic}} = \frac{1}{2} E\varepsilon_{\mathrm{p}}^2 \Delta x(k_{\mathrm{r}} - 1), \tag{4}$$

where Δx is the length of the element bar (DEM grid size) and $k_{\mathrm{r}} = \varepsilon_{\mathrm{r}}/\varepsilon_{\mathrm{p}}$ (Fig. 5a) is the coefficient that defines strain softening (after the peak stress has been reached until the crack totally opens). The critical tensile stress, σ_{c}, is calculated by use of a modified classical Griffith (1920) equation:

$$\sigma_{\mathrm{c}} \cong \sqrt{\frac{EG_{\mathrm{Ic}}}{\pi c}}, \tag{5}$$

where $2c$ is the pre-existing crack length. For a crack in a linear elastic solid, G_{Ic} is expressed in terms of the critical stress intensity factor, K_{Ic}, in mode I. From Griffith's energy balance concept, it follows that

$$G_{\mathrm{Ic}} = \frac{K_{\mathrm{Ic}}^2(1 - \nu^2)}{E}. \tag{6}$$

From equations (5) and (6), the critical stress intensity factor, K_{Ic}, is

$$K_{\mathrm{Ic}} = \chi\sigma_{\mathrm{c}}\sqrt{L}. \tag{7}$$

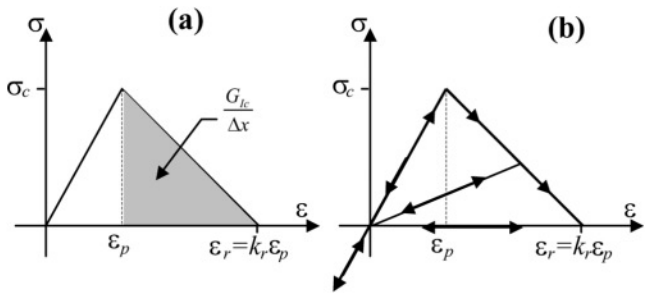

Figure 5. (a) Constitutive relation for tensile crack generation used in the DEM, and (b) the loading–unloading path of the stress on each bar; it is actually the stress-strain constitutive relation for one bar before and after the bar breaks.

In the problem under consideration, L is the length of the pre-existing fault and χ a nondimensional factor that depends on the geometry and grid size of the DEM. Equations (3), (6), and (7) verify that

$$\varepsilon_{\mathrm{p}} = \frac{1}{\chi}\sqrt{\frac{G_{\mathrm{Ic}}}{(1 - \nu^2)LE}}. \tag{8}$$

The nondimensional factor, χ, is estimated by combining equations (4) and (8), giving

$$\chi = \sqrt{\frac{(k_{\mathrm{r}} - 1)\Delta x}{2(1 - \nu^2)L}}, \quad k_{\mathrm{r}} > 1. \tag{9}$$

For the tensile crack propagation formulation, two parameters from a set of alternatives must be previously defined; the critical tensile stress intensity factor, K_{Ic} (or the critical tensile fracture energy, G_{Ic}), and the k_{r} coefficient.

Estimation of Dynamic Parameters for the 2000 Tottori Earthquake

For the 3D shear dynamic spontaneous rupture simulation of a real earthquake, we need to know the geometry of the fault, the initial stres distribution along the fault, the stress drop distribution, the strength of the fault, and the critical slip, D_{c} (if the slip-weakening friction model is used). The choice of these parameters is a delicate issue, still a subject of debate. Assuming that the effective stress causing slip is the stress drop, the absolute stress value is not necessary. The initial stress therefore could be assumed to be at a zero level. Then, under this assumption, we need to define the stress drop, the strength excess, and the critical slip along the fault. These parameters could be estimated from the shear stress function that changes in time during an earthquake, as schematically shown in Figure 6a. But the direct estimation of the shear stress change from observations is not feasible. The closest information about the source presently available is the results of the kinematic waveform in-

version given by the slip distribution in time (Fig. 6b) along the fault. In this context, for the computation of the shear stress change during earthquake rupture, we used the distribution of fault slip and rupture time obtained from the inversion of strong motion waveforms. For this purpose, using the DEM, we modeled the continuum surrounding the pre-existing fault as specified by the kinematic model and solved the elastodynamic equation of motion for a rupture along the fault plane. The slip distribution in space and time obtained by the kinematic fault model was used as a boundary condition along the pre-existing fault. This allows the determination of the relative stress time history (Fig. 6a) at every nodal point along the fault. This procedure, that is, determination of the dynamic stress change from the results of kinematic waveform inversion, has been used by several authors (e.g., Quin, 1990; Miyatake, 1992; Mikumo and Miyatake, 1995; Bouchon, 1997; Day *et al.*, 1998; Mikumo *et al.*, 1999; Dalguer *et al.*, 2002), most of them using the finite difference method. From the results of the stress-time function (Fig. 6a), the strength excess and the dynamic and static stress drops may be estimated. From the expression of the stress as function of the slip (as observed schematically in Fig. 6c), the critical slip could be roughly estimated.

Until now, four different source models of the 2000 Tottori earthquake have been obtained from kinematic inversion: (1) by Iwata *et al.* (2000) from near-source strong motion waveforms (first version), (2) by Sekiguchi and Iwata (2001) from near-source strong motion records and GPS and leveling data (second version) (this model was based on the multiple-segment fault model of Fukuyama *et al.* [2001]), (3) by E. Fukuyama and D. S. Dreger (unpublished manuscript, 2001) from regional broadband seismic waveforms, and (4) by Yagi (2001) from near-source strong motion data and teleseismic waveform. In our study we refer to the first version of Iwata *et al.*'s (2000) slip model. This model was chosen because of its simplicity (one segment fault), which satisfies the requirement of the present study.

In a previous publication (Dalguer *et al.*, 2002), we estimated the dynamic and static shear stress changes for the 2000 Tottori earthquake, following the procedure described earlier, using the distribution of fault slip obtained from the inversion of strong motion waveforms calculated by Iwata *et al.* (2000). In the present article, we used these results and refined the model for a grid size of 0.5 km. We adopted the fault-plane properties defined by Iwata *et al.* (2000), that is, a fault plane with strike N150°E and dip 90° and a fault length and width of 33 km and 21 km. The hypocenter was located at a depth of 13.4 km. The velocity structure is shown in Table 1. The result is summarized in Figure 7, in which the dynamic stress drop, strength excess, and critical slip distributions are shown. From Figure 7a we may conclude that the causative fault of the 2000 Tottori earthquake had a very heterogeneous stress distribution, with a localized asperity in the upper central part of the fault. The maximum stress drop is 30 MPa in the asperity zone. The strength excess distribution along the fault (Fig. 7b) shows maximum values (around 5 MPa) at the left and right sides of the fault. The critical slip distribution along the fault (Fig. 7c) was approximately estimated from the zone in which the stress has positive stress drop. The estimated values of D_C tend to vary with depth, being on average 2.0 m near the free surface, 1.0 m at the center of the fault, and 0.4 m at the deepest zone. However, it looks that an equally good interpretation would be that D_C varies in rough proportion to the total slip. It is important to remark that the way we estimated D_C could produce artificial slip-weakening relations (due probably to the finite grid size and time increment), as shown by Ide and Takeo (1997). But the choice of D_C values is quite difficult, since there is no way to get them directly from observation and there may be various combinations that fit the data. This is in accordance with the conclusion from Guatteri and Spudich (2000), who indicated that there is no unique solution to select D_C. The recent approach of Mikimo *et al.* (2003), in which the time peak slip velocity of the kinematic model approximately corresponds to the time of the slip-weakening distance, looks more appropiate because it is based in a physically based relation between the breakdown time of shear stress, the time of peak slip velocity, and the slip-weakening distance D_C from the time histories of shear stress, slip, and slip velocity at each point on the fault. But they also mentioned that this idea depends on a very good resolution in

Table 1
Velocity Structure

Depth (km)	V_p (km/sec)	V_s (km/sec)	ρ (kg/m^3)
0	5.5	3.179	2600
2	6.05	3.497	2700
16	6.6	3.815	2800
38	8.03	4.624	3100

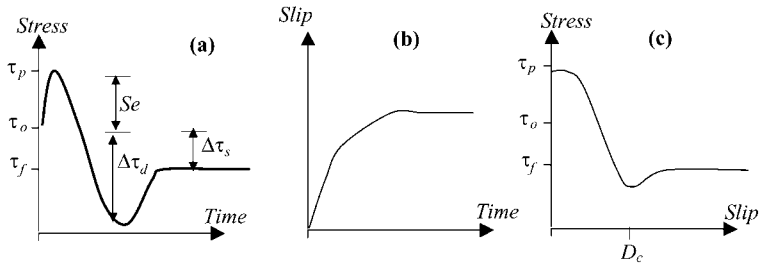

Figure 6. Characteristics of shear stress and slip function on any discrete point of a fault and dynamic parameter specification: (a) shear stress time history; (b) slip time function; and (c) shear stress versus slip function, where τ_p = peak shear stress, τ_o = initial shear stress, τ_f = final shear stress, $\Delta\tau_d$ = dynamic stress drop, $\Delta\tau_s$ = static stress drop, S_e = strength excess, and D_C = critical slip.

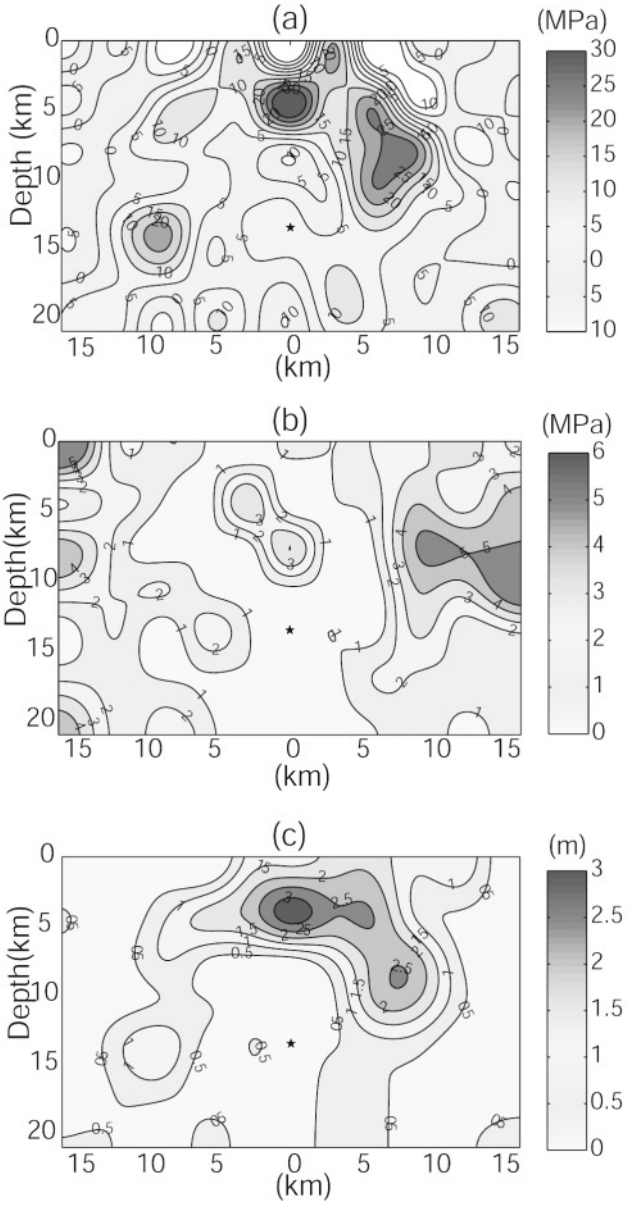

Figure 7. Dynamic parameter distribution along the fault estimated from the results of the kinematic source model of Iwata *et al.* (2000) of the 2000 Tottori earthquake: (a) dynamic stress drop distribution; (b) strength excess distribution along the fault; (c) critical slip distribution.

time of slip velocity of the kinematic model (around 40 time windows for the kinematic inversion are needed). Then, the estimations of D_C values for real earthquakes are very complex and there are many uncertainties. Since we estimated the D_C values directly from the kinematic slip model, we believe that these results reflect in general the appropriate D_C distribution for the model used. Kinematic source slip models are the best information we have from the source. Therefore, they are the best starting point for estimating dynamic parameters and developing dynamic models.

Dynamic Fault Model

In order to simulate the surface rupture, as shown in Figure 2, we assumed that the pre-existing fault, defined by the kinematic model (Iwata *et al.*, 2000), is embedded at a depth of 2.0 km from the free surface. The model used for the simulation was a solid body with dimensions 117 km × 117 km × 40 km. For this model, 4,380,480 cubic cells with 0.5-km-long sides were needed. For the dynamic shear stress rupture simulation, the dynamic stress-drop distribution (Fig. 7a) and the strength excess (Fig. 7b) were used. For the critical slip (D_C) distribution, the values given by Figure 6c were used, but with the assumption that a maximum D_C = 2.0 m is permitted (for simulations with D_C values greater than 2.0 m, we got very low frequency ground motion, which was not consistent with the observation records). For the generation of the tensile cracks, we assumed that the critical fracture energy in mode I, G_{Ic}, changes with depth according to the velocity structure given in Table 1. That is, for the first layer $G_{Ic} = 10 \times 10^5$ J/m^2, for the second layer $G_{Ic} = 4 \times 10^5$ J/m^2, and for the third layer $G_{Ic} = 3 \times 10^5$ J/m^2. The coefficient $k_r = 1.5$ was assumed to be constant (see equation 9). These parameters were chosen to control the number of tensile cracks and to produce a clear crack-formation pattern. For very low G_{Ic} values, the medium around the pre-existing fault would be completely filled with cracks, making it difficult to distinguish the crack pattern. In contrast, at very high values no cracks are generated. Some authors (e.g., Atkinson, 1987) have suggested that G_{Ic} could be 1/10 to 1/100 smaller than the shear fracture energy. We tried to keep this interval.

Simulated Tensile Crack Distribution and Surface Rupture

The final distribution of new tensile cracks is presented in Figures 8–11. The broken bars of the DEM are represented as discrete cracks (in the figures they are dots located at the center of each bar) that clearly form the pattern of the new surface of cracks. Figure 8 shows views of the final stage of development of new cracks from both sides of the fault. The cracks grow from the two sides of the fault, following different patterns and forming a complex flowerlike structure pattern. Besides the natural asymmetry of the tensile stress across the fault, the heterogeneity of the fault contributes to the complexity of the crack pattern. As depicted by Figure 9a,c, in which bird's-eye and line cross-sectional views of the fault are presented, the global view of all the cracks across the pre-existing fault is very complex. From these figures and from the frontal view of Figure 9b, the tensile cracks are generated mainly from the asperity zone (area of highest values of stress drop) and from the top of the fault. We attribute the complexity of the cracks not only to the natural asymmetry of the tensile stress across the fault, as predicted in our previous article (Dalguer *et al.*, 2003) (where we simulated the crack evolution of pure strike-slip

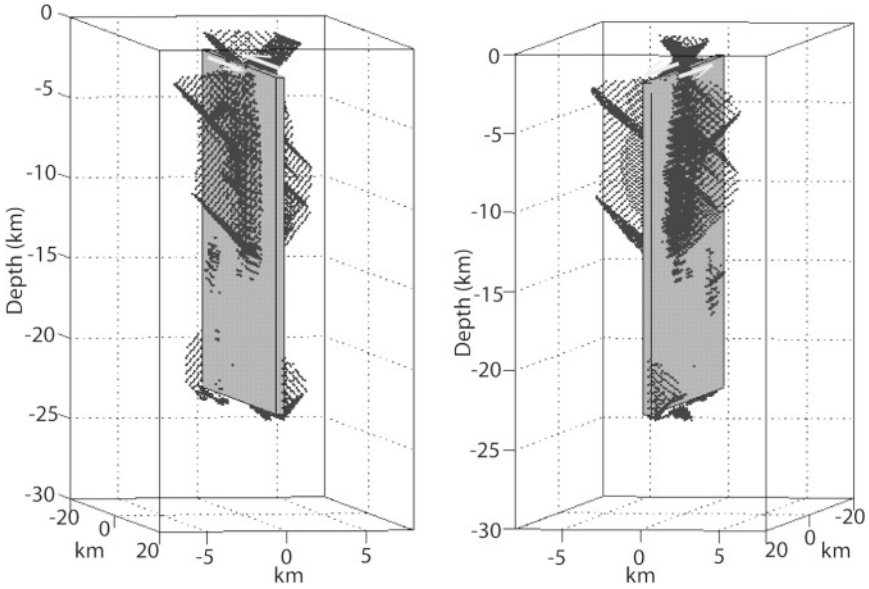

Figure 8. Two perspectives of the final stage of crack evolution for the 2000 Tottori earthquake dynamic simulation. The gray surface represents the shear crack on the pre-existing fault, and the dashed lines represents the tensile cracks.

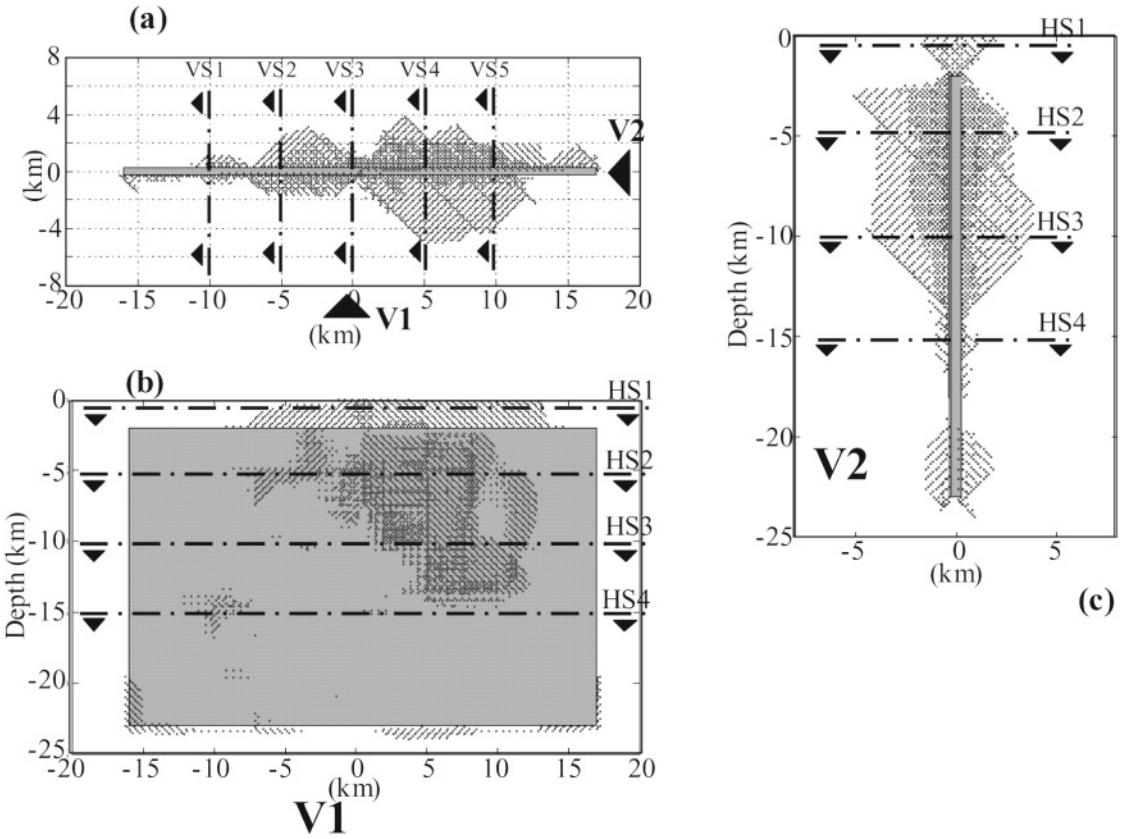

Figure 9. Views of the final stage of crack evolution for the 2000 Tottori earthquake dynamic simulation: (a) bird's-eye view; (b) frontal view (V1); (c) line cross-sectional view (V2).

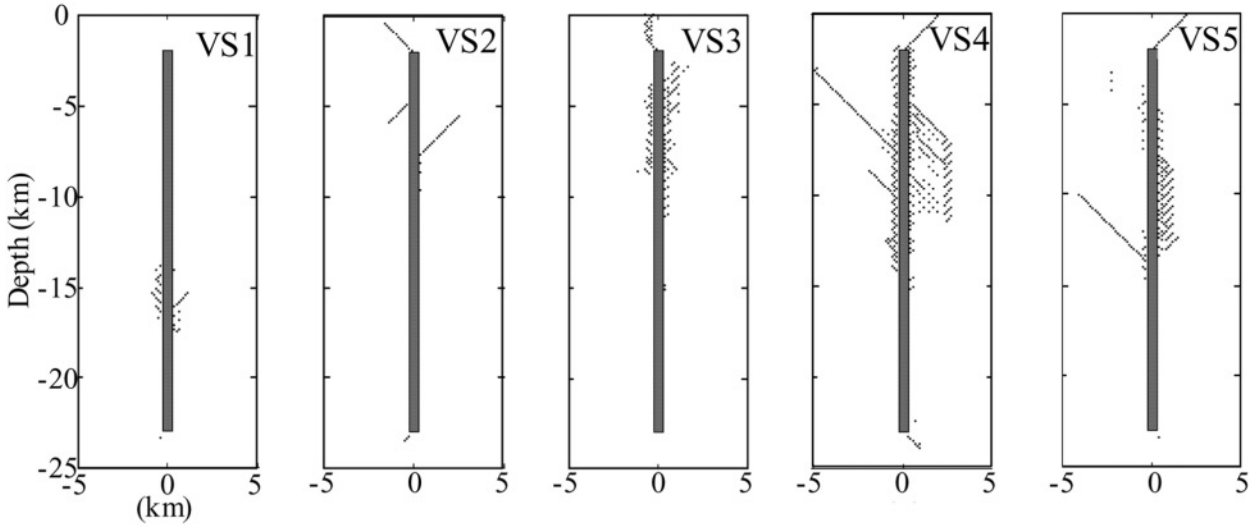

Figure 10. Vertical cross sections VS1, VS2, VS3, VS4, and VS5 of the final stage of crack evolution for the 2000 Tottori earthquake dynamic simulation. The location of these sections is specified in Figure 9a. The vertical thick line is the pre-existing shear fault.

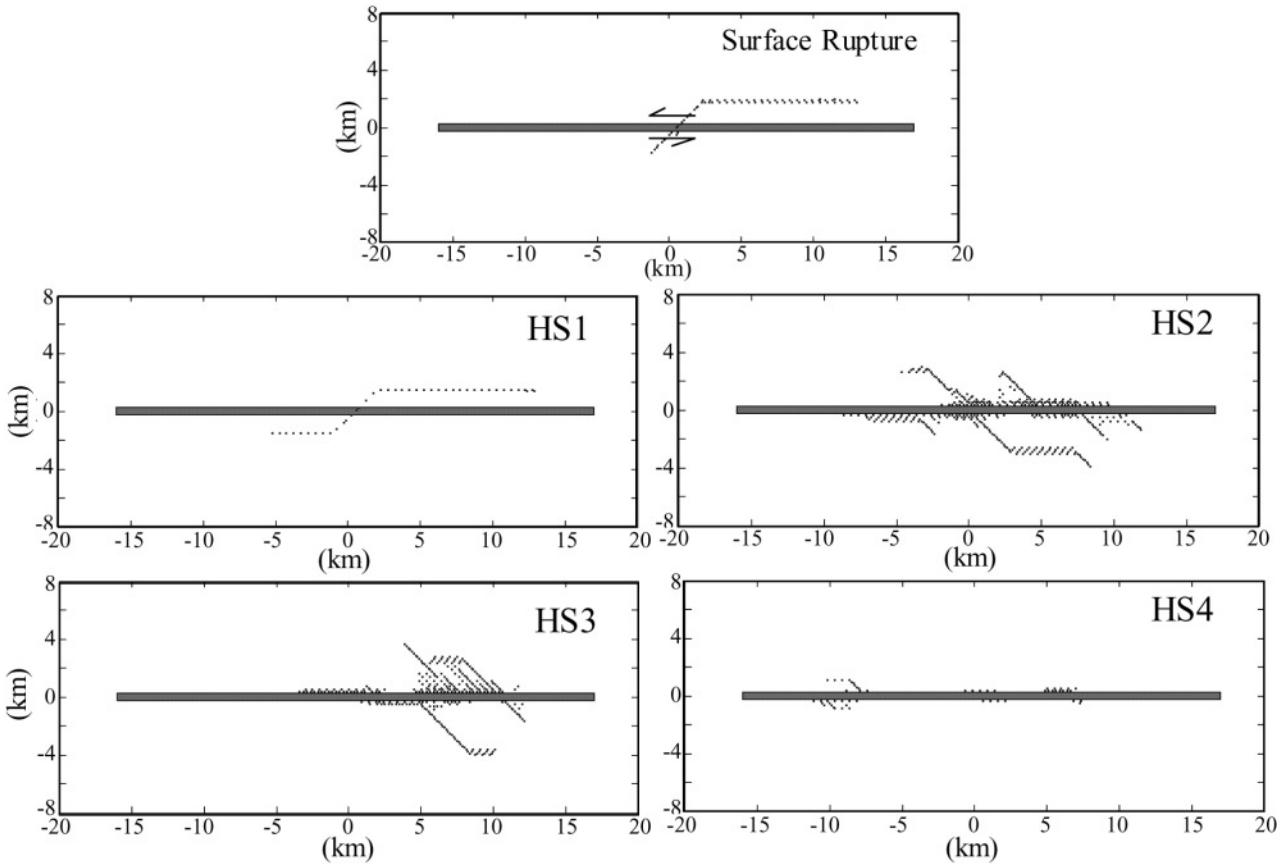

Figure 11. Surface rupture and horizontal cross sections HS1, HS2, HS3, and HS4 of the final stage of crack evolution for the 2000 Tottori earthquake dynamic simulation. The location of these sections is specified in Figure 9b,c. The horizontal thick line is the pre-existing shear fault.

faults with homogeneous stress distribution), but also to the heterogeneity of stress and strength distribution along the fault.

Details of the characteristics of these complex cracks formed as a flowerlike structure are seen in the vertical cross sections (VS1, VS2, VS3, VS4, and VS5) shown in Figure 10. The locations of these sections are specified in Figure 9a. Section VS1, located in a zone of low stress drop, shows few cracks. From the right side of section VS2 and left side of VS4, one main crack develops at a depth of about 7.5 km and extending toward the free surface. Two main cracks develop from the left side of VS2 and right side of VS4; one originates at around 5.0 km depth and extends downward, whereas the other originates at the top of the fault and grows toward the free surface. This second one, in section VS4, reaches the free surface, whereas in VS2 the crack stops very close to the surface. The development of cracks springing from the bottom of the fault may be observed in both sections. The cracks originating in section VS4 extend a longer distance than those originating in section VS2. Section VS4 also shows the development of more cracks than in VS2. Note that section VS4 is located in the main zone of the asperity, which explains the differences observed. Section VS3, located in the middle of the fault, shows shorter cracks originating mainly along the asperity and top of the fault. Section VS5 shows two main cracks, one originating at around 14.0 km depth (left side) and the other (right side) at the top of the fault, both growing toward the free surface. The crack originating from the top of the fault reaches the free surface.

The surface rupture and horizontal cross sections (HS1, HS2, HS3 and HS4) are shown in Figure 11. The location of these sections is specified in Figure 9b,c. The main characteristic of the pattern is that the new cracks extend from the asperity asymmetrically from the two sides of the fault. The faulting generates a surface rupture on only one side of the fault about 10.0 km long, parallel to the trace of the main fault and at a distance of 2.0 km. This surface rupture crosses to the other side of the fault at its center. Section HS1, located at a 0.75 km depth from the free surface, shows cracks parallel to the fault on the two sides of the fault. The surface rupture and the cracks from section HS1 correspond to the flowerlike structure generated from the top of the fault. Sections HS2 and HS3, located at 5.0 and 10.0 km depth, respectively, cross the main part of the asperity zone. The cracks occur in an opposite pattern compared with section HS1. Section HS4, located at 15.0 km depth and outside of the asperity, shows a few cracks.

On the basis of these results, tensile rupture patterns appear to grow only at angles of 45° and $-45°$. This suggests that maximum tensile stress occurs in this zone. The geometrical form and grid size of each DEM element may constitute a limitation such that no cracks grow at any other angles. However, in Dalguer *et al.* (2003), the 45° did not seem as pronounced when we simulated tensile cracks in a theoretical 2D problem. It indicates that this is not an inherent problem with the method. Therefore, in spite of this possible limitation, the results presented in the present article can still give a valid indication of tensile crack generation.

Comparison of the Tensile Crack Simulated with Observation and Aftershock Distribution

As mentioned in the Introduction, during the field observations reported by Fusejima *et al.* (2000) after the 2000 Tottori (Japan) earthquake, several cracks were observed on the free surface parallel to the causative fault. Some of these cracks may correspond to the flowerlike structures originating during the rupture process of the Tottori earthquake. The surface rupture simulated in the previous section is similar to some of the traces of the cracks observed in the field, as shown by Figure 12. It suggests that the tensile cracks may have been generated mainly along the central part of the fault.

The hypothesis of the development of a flowerlike structure is supported by the seismic reflection survey around the 2000 Tottori (Japan) earthquake area performed by Inoue *et al.* (2001), as shown in Figure 3 and by the tomographic slices of *P*-wave velocity at different depths (Fig. 13) developed by Abe *et al.* (2001). The first two images (0.0 and 2.0 km) of this figure show strong discontinuity of P-wave velocity. The red color, which represents very low values, is located in a zone around the causative fault. From our interpretation, this zone is a weakness area and may be a fractured zone.

The new surface cracks could form in a plane of shear failure after or during the earthquake. It could be plausible because these zones are weakness planes and they are under tectonic stresses. After a certain time when stress is accumulated along these weakness planes, shear slip can occur. It suggests that these new surfaces may be the zone of aftershocks. In Figure 14 we find that some of the cracks are associated with the aftershock distribution. In Figure 14a, showing a bird's-eye view of the aftershock distribution, a cluster of events may be observed following approximately the traces as specified by the white line. This part of the aftershocks may be related to the cracks of section HS1 and HS2, as shown in Figure 14a. The vertical view (section VV′) of the aftershock distribution (Fig. 14b) might be associated to the cross section VS4 and VS5 and the line cross-sectional view V2 (see Fig. 9c) of crack distribution as shown in Figure 14b. If these cracks correspond to the zone of aftershocks, the cracks simulated could have been extended and be larger during the real earthquake, as specified with the dashed line in the vertical view (section VV′) of the aftershock distribution (Fig. 14b).

In order to validate the dynamic simulation studied here, the simulated waveform was compared with the ground motions recorded by the Kiknet and Knet. For comparison, the simulated waveform and the seismic records were filtered in a frequency range between 0.05 and 0.5 Hz. Figure 1 shows the location of all the stations of seismic record used for comparison. Figures 15 and 16 show the comparison with

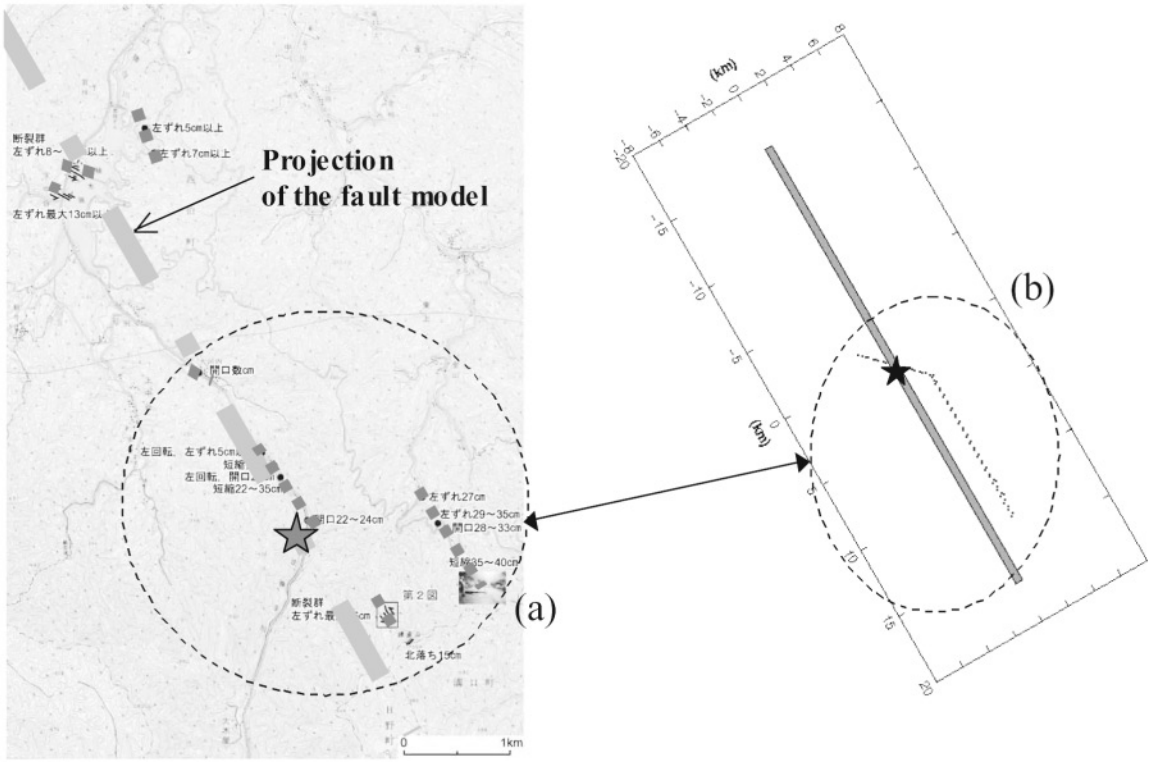

Figure 12. Surface rupture observed by Fusejima *et al.* (2000) in the field (a) associated with the surface rupture simulated (b).

the observation. In general, the simulation fits the observation well. Even though the purpose of the proposed mode is not to simulate synthetic seismograms that fit the observed records, to do that tensile cracks are certainly not necessary, because it is very well accepted that the earthquake is a dynamically running shear crack, so the mode II and III cracks are the most important factors for the generation of seismic energy, ground motion, and shaking; we developed an additional model without tensile cracks in order to see how different the synthetic seismogram would be without including the cracks. From the results, as shown in Figures 17 and 18, in general the synthetic seismograms fit the observed records equally well. At some stations, such as the up–down component of station SMN001, north–south of SMN003, north–south of TTR007 (Figs. 15 and 17), and north–south of SMND02 (Fig.16 and 18), the model with tensile cracks has a better fit than the model without tensile cracks. Another difference between these two models is that the model with cracks tends to generate shorter wavelengths than the model without cracks. These results suggest that the model with cracks predicts ground motions with higher frequency content than the model without cracks.

Conclusions

To our knowledge, this article contains the first numerical 3D simulation of the generation of tensile cracks by the dynamic shear rupture process along a pre-existing fault during a real earthquake.

From the simulation results, we can conclude that during the dynamic shear rupture process of the 2000 Tottori earthquake, tensile cracks were generated. Some of these cracks reached the free surface. The assumption that the fault is embedded at a depth of 2.0 km from the surface allowed us to simulate some of the surface ruptures observed in the field after the Tottori earthquake. The results show that the simulated shear rupture process generates tensile cracks that reach the free surface on only one side of the fault, in a direction parallel to the trace of the main fault and at a 2.0-km distance from the fault. The trace of this surface rupture coincides to some of the several cracks observed on the field by Fusejima *et al.* (2000). It may be seen that the new cracks grow from the two sides of the fault, following different patterns and forming new fractures as a complex flowerlike structure. We attribute the complexity of the cracks not only to the natural asymmetry of the tensile stress across the fault, but also to the heterogeneity of stress and strength distribution along the fault. The new cracks grow mainly from the asperity zone (area of highest values of stress drop) and from the top of the fault. Some of the new cracks are also associated with the aftershock distribution, suggesting that some of the cracks opening during the shear rupture could be zones of potential aftershocks.

It is difficult to say weather these simulated cracks are

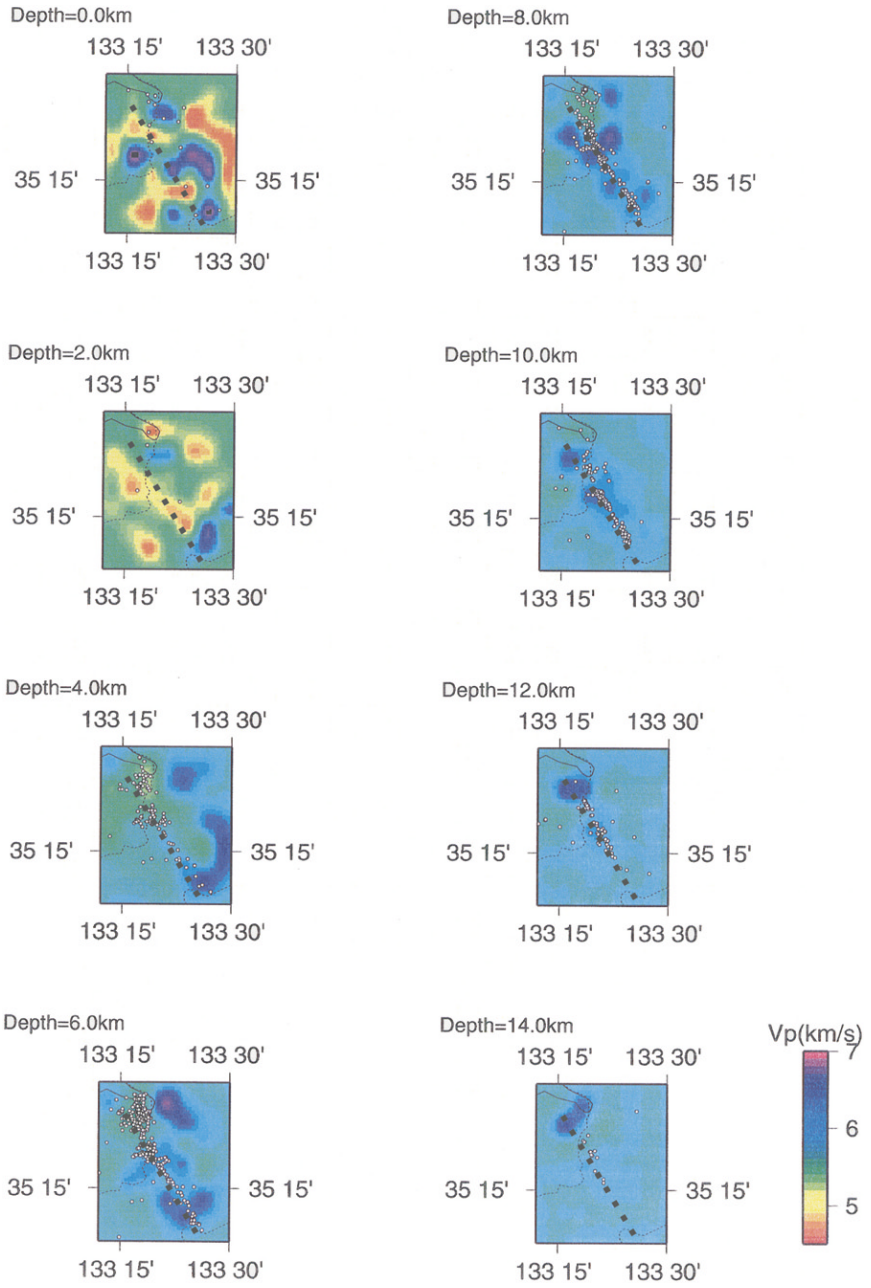

Figure 13. Tomographic slices developed by Abe *et al.* (2001) at different depths showing *P*-wave velocity and aftershock distribution of the 2000 Tottori earthquake. The first two images (0.0 and 2.0 km) suggest the existence of a flower structure near the free surface because of the strong discontinuity of lower values of *P*-wave velocity in the localized zone around the causative fault. The dashed line is the projection of the trace of the causative fault of the 2000 Tottori earthquake.

real or not. But the crack observed on the ground, the analysis of seismic profile, and the association with aftershock distribution suggest a fractured zone near the free surface. These observations are consistent with the simulated cracks presented in this article.

In order to validate the dynamic simulation of the Tottori earthquake presented here, the simulated waveforms were compared with the ground motions recorded by Kiknet and Knet. In general, the simulations fit well the observations in a frequency range from 0.05 to 0.5 Hz.

We can conclude that the proposed technique for the numerical analysis of the full dynamic rupture process including the generation of tensile cracks during an earthquake leads to truly encouraging results. The model and the results presented in this article show that our approach will be used successfully in predicting near-source ground motion, frac-

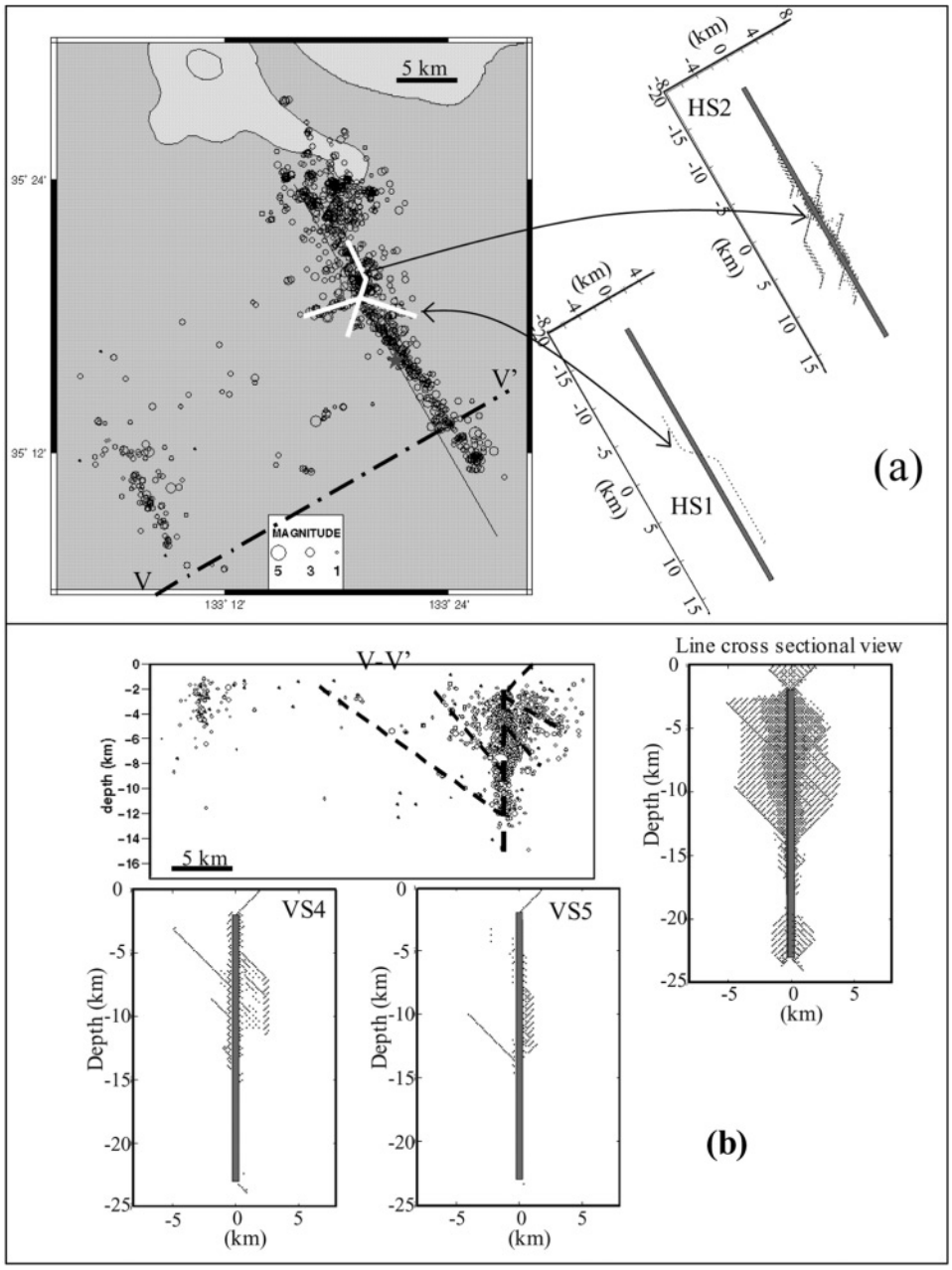

Figure 14. Aftershock distribution, determined by Shibutani *et al.* (2002), associated with the simulated cracks: (a) bird's-eye view of aftershock associated with the horizontal section HS1 and HS2 of cracks (see Fig. 11). (b) Vertical distribution (section VV′) of aftershock associated with the line cross-sectional view V2 (see Fig. 9c) and vertical cross sections VS4 and VS5 of crack distribution (see Fig. 10). The dashed lines of section VV′ represent the projection of possible cracks deduced from the aftershock distribution.

ture behavior during an earthquake, and the formation of new fault zones.

Acknowledgments

This article was supported by the Special Coordination Funds for Promoting Science and Technology titled "Study on the master model for strong ground motion prediction toward earthquake disaster mitigation," the Grant-in-Aid for Science Research number 14002116, and the research grant awarded by the Japan Society for the Promotion of Science (JSPS) under "FY2002 JSPS Postdoctoral Fellowship for Foreign Researchers" from the Ministry of Education, Science, Sports, and Culture of Japan. We also would like to thank to Dr. Shibutani and Dr. Katao for providing us detailed information of the aftershock distribution of the 2000 Tottori earthquake. Thanks to Dr. Iwata for providing us with the kinematc fault-slip model of the 2000 Tottori earthquake and to Dr. Abe for providing us the figures of the study of seismic reflection survey around the 2000 Tottori

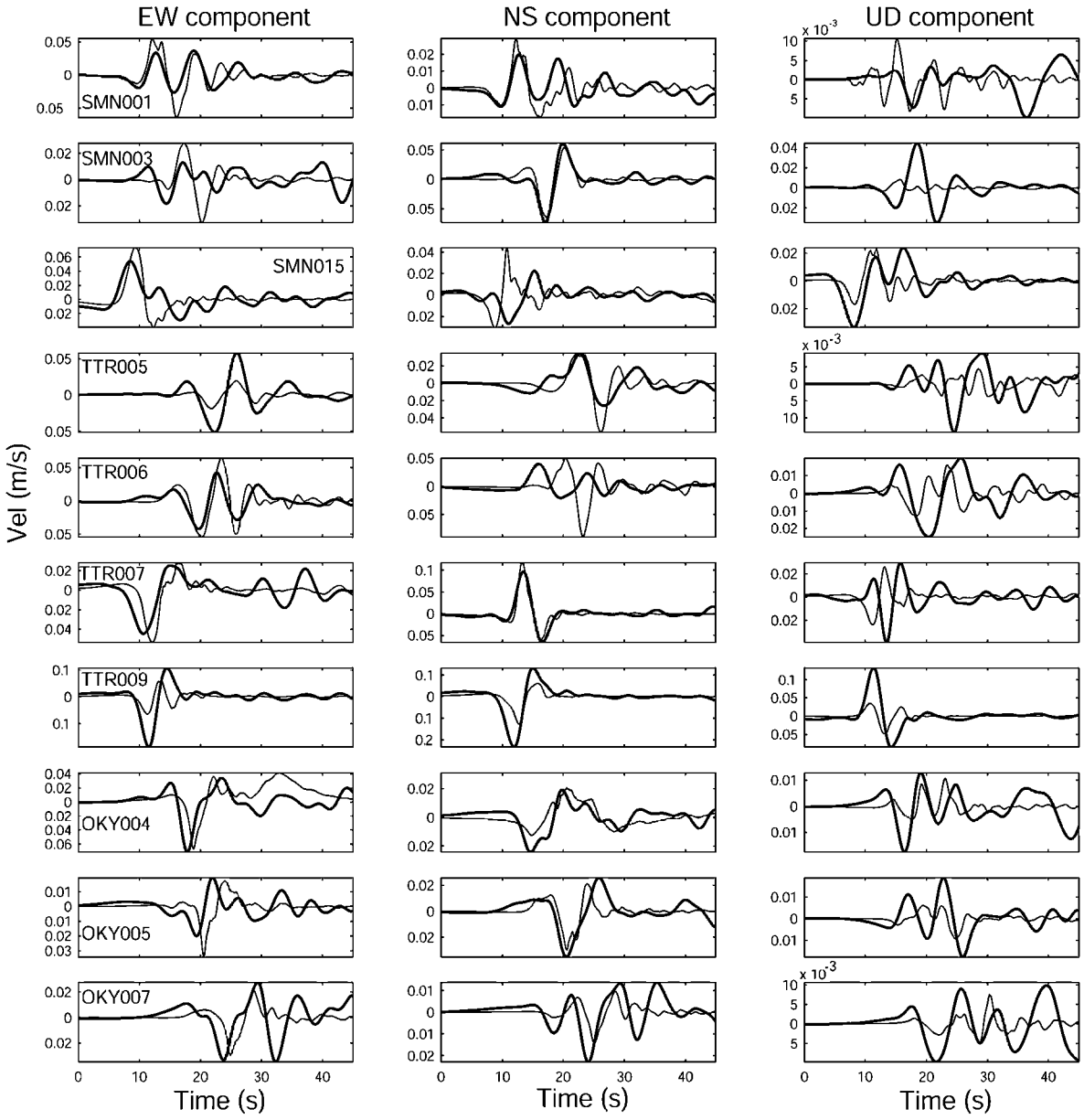

Figure 15. Dynamic model with tensile cracks. Comparison of the velocity ground-motion simulation with stations records of Knet in the frequency range of 0.05–0.5 Hz. The thick line is the simulation, and the thin line is the recorded event. Figure 1 shows the location of all the stations used for comparison.

(Japan) earthquake area developed by Inoue *et al.* (2001). Finally, we express our sincere thanks to the reviewers, Prof. Steve Day and an anonymous reviewer and the associate editor, David D. Oglesby, for constructive reviews and valuable suggestions.

References

Abe, S., K. Miyakoshi, and D. Inoue (2001). Seismic reflection survey around the 2000 Tottori-Ken earthquake area, 2001 Japan Earth and Planetary Science Joint Meeting. S3-P013, 4–8 June 2001, Tokyo, Japan.

Anders, M. H., and D. V. Wiltschko (1994). Microfracturing, paleostress, and the growth of faults, *J. Struct. Geol.* **16,** 795–815.

Andrews D. J. (1976). Rupture velocity of plane-strain shear cracks, *J. Geophys. Res.* **81,** 5679–5687.

Atkinson, B. K. (1987). *Fracture Mechanics of Rock*, Academic, New York.

Bouchon, M. (1997). The state of stress on some faults of the San Andreas system as inferred from near-field strong motion data, *J. Geophys. Res.* **102,** 11,731–11,744.

Cox, S. J. D., and C. H. Scholz (1988). Rupture initiation in shear fracture of rocks: an experimental study, *J. Geophys. Res.* **93,** 3307–3320.

Dalguer, L. A. (2000). Simulação de movimentos sismicos considerando o mecanismo de ruptura da falha causativa do terremoto, *Ph.D. Thesis*, Federal University of Rio Grande do Sul, Porto Alegre R.S., Brazil (in Portuguese).

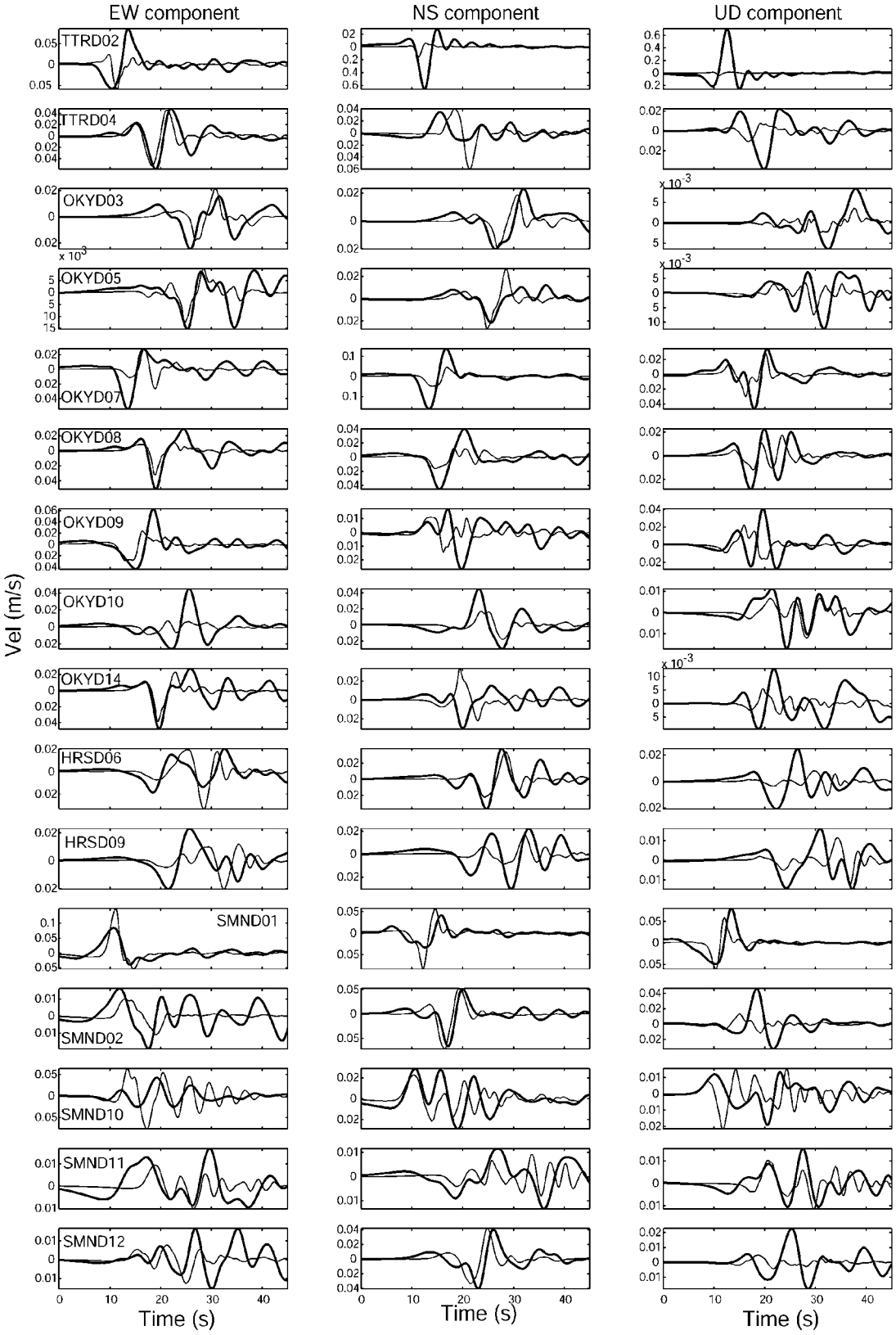

Figure 16. Dynamic model with tensile cracks. Comparison of the velocity ground motion simulation with stations records of Kiknet in frequency range of 0.05–0.5 Hz. The thick line is the simulation, and the thin line is the recorded event. Figure 1 shows the location of all the stations used for comparison.

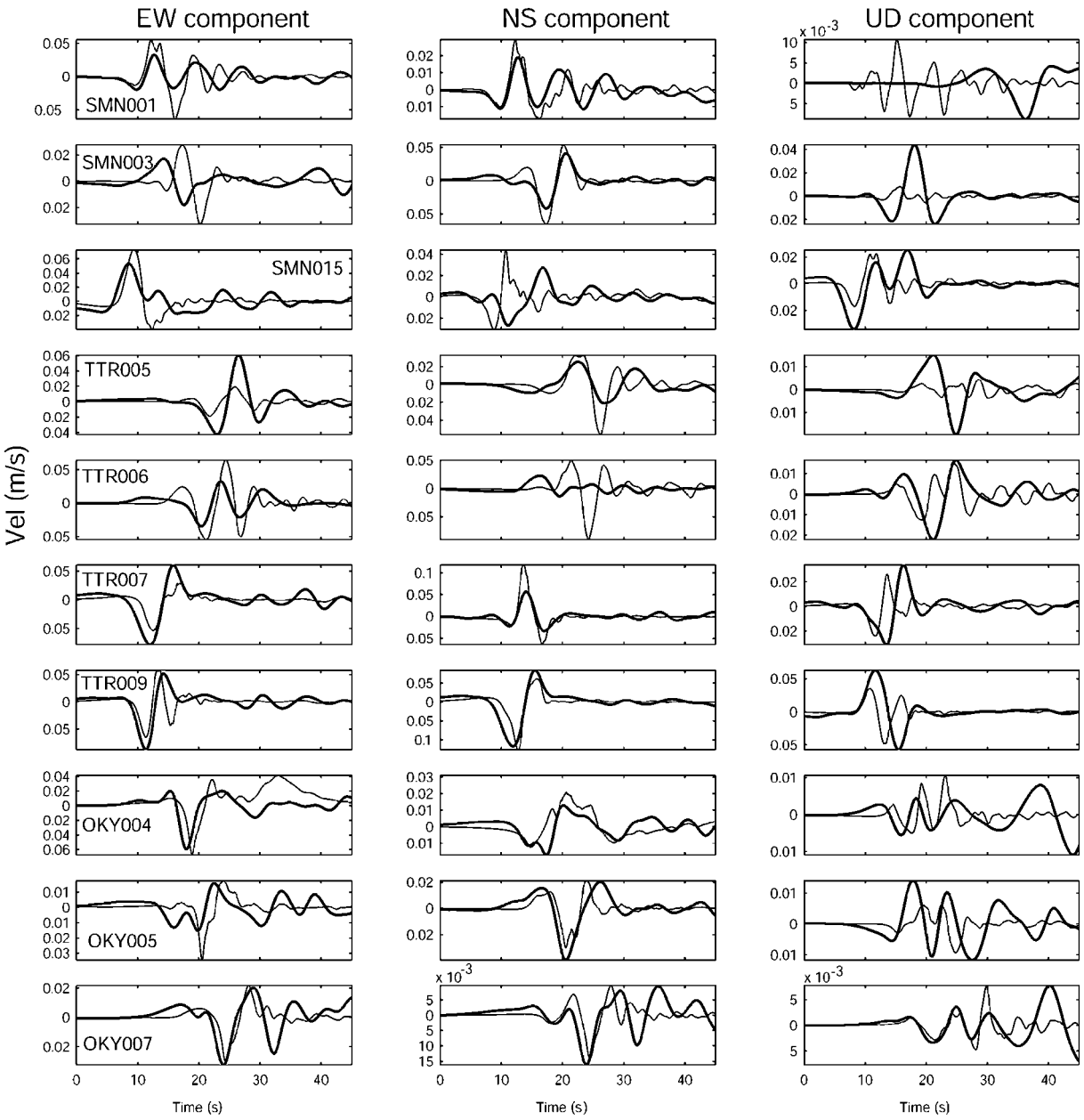

Figure 17. Dynamic model without tensile cracks. Comparison of the velocity ground-motion simulation with stations records of Knet in the frequency range of 0.05–0.5 Hz. The thick line is the simulation, and the thin line is the recorded event. Figure 1 shows the location of all the stations used for comparison.

Dalguer, L. A., K. Irikura, J. Riera, and H. C. Chiu (2001a). Fault dynamic rupture simulation of the hypocenter area of the thrust fault of the 1999 Chi-Chi (Taiwan) earthquake, *Geophys. Res. Lett.* **28,** 1327–1330.

Dalguer, L. A., K. Irikura, J. Riera, and H. C. Chiu (2001b). The importance of the dynamic source effects on strong ground motion during the 1999 Chi-Chi, Taiwan, earthquake: brief interpretation of the damage distribution on buildings, *Bull. Seism. Soc. Am.* **95,** 1112–1127.

Dalguer, L. A., K. Irikura, W. Zhang, and J. Riera (2002). Distribution of dynamic and static stress changes during 2000 Tottori (Japan) earthquake: brief interpretation of the earthquake sequences—foreshocks, main shock, and aftershocks, *Geophys. Res. Lett.* **29,** no. 16, 1758, doi 10.1029/2001GL014333.

Dalguer, L. A., K. Irikura, and J. Riera (2003). Simulation of tensile crack generation by 3D dynamic shear rupture propagation during an earthquake, *J. Geophys. Res.* **108,** no. B3, 2144, doi 10.1029/2001JB001738.

Day, S. M. (1982). Three-dimensional simulation of spontaneous rupture: the effect of nonuniform prestress, *Bull. Seism. Soc. Am.* **72,** 1881–1902.

Day, S. M., G. Yu, and D. J. Wald (1998). Dynamic stress change during earthquake rupture *Bull. Seism. Soc. Am.* **88,** 512–522.

Fukuyama, E., and R. Madariaga (1998). Rupture dynamic of a planar fault in a 3D elastic medium: rate- and slip-weakening friction, *Bull. Seism. Soc. Am.* **88,** 1–17.

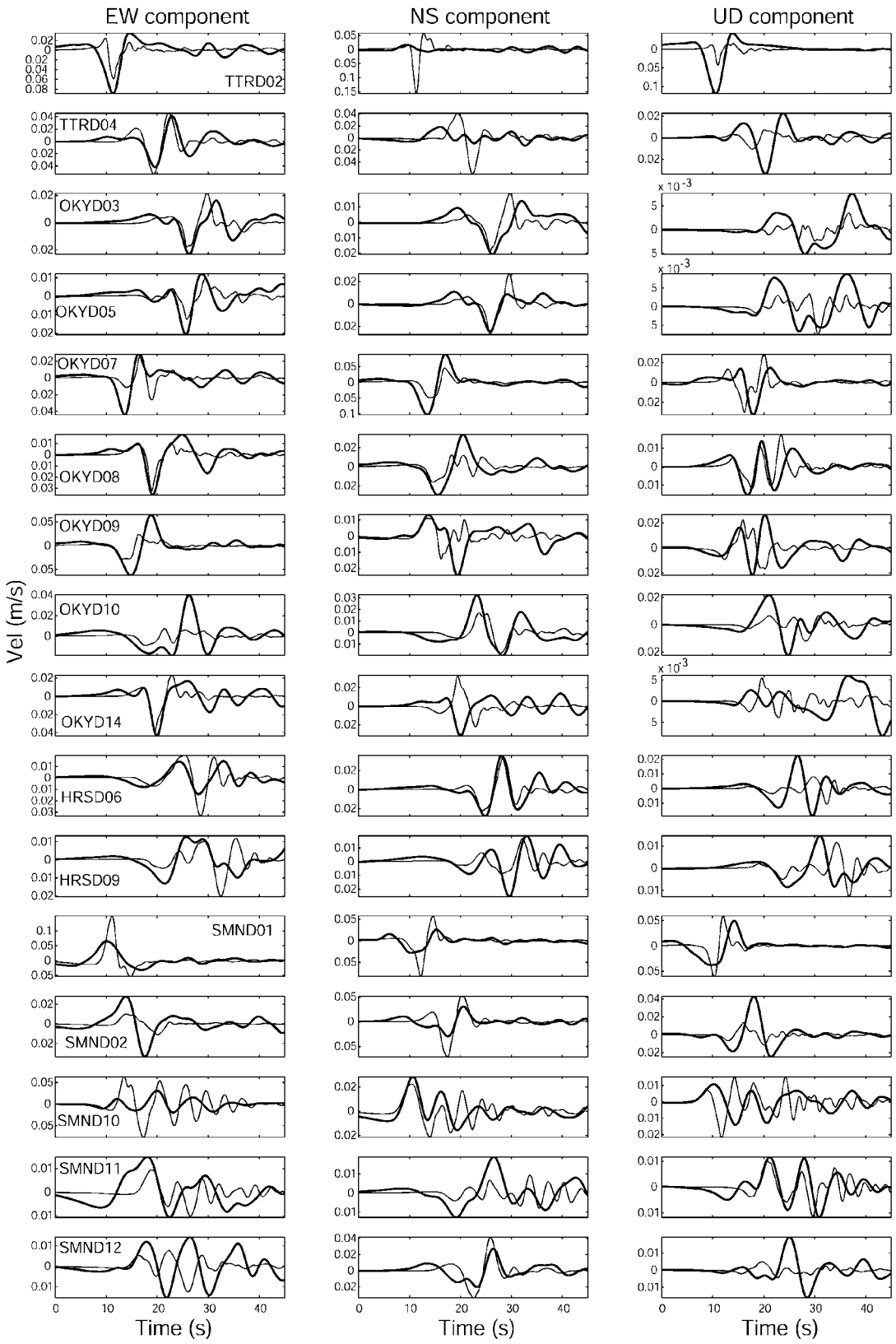

Figure 18. Dynamic model without tensile cracks. Comparison of the velocity ground-motion simulation with stations records of Kiknet in frequency range of 0.05–0.5 Hz. The thick line is the simulation, and the thin line is the recorded event. Figure 1 shows the location of all the stations used for comparison.

Fukuyama, E., W. L. Ellsworth, F. Waldhauser, and A. Kubo (2001). Very fine fault structure of the 2000 western Tottori, Japan, earthquake, Presented at the Japan Earth and Planetary Science Joint Meeting, S3-007 June 2001, Tokyo, Japan.

Fusejima, Y., T. Yoshioka, K. Mizuno, M. Shishikura, R. Imura, T. Komatsubara, and T. Sasaki (2000). Surface rupture associated with the 2000 Tottori-ken Seibu earthquake, Annual Report on Active Fault and Paleoearthquake Researches, No. 1, Geological Survey of Japan, National Institute of Advanced Industrial Science and Technology.

Griffith, A. A. (1920). The phenomena of rupture and flow in solids, *Phil. Trans. R. Soc. A*, **221,** 163–198.

Guatteri, M., and P. Spudich (2000). What can strong-motion data tell us about slip-weakening fault-friction laws? *Bull. Seism. Soc. Am.* **90,** 98–116.

Harris, R. A., and S. M. Day (1999). Dynamic 3D simulations of earthquakes on en echelon faults, *Geophys. Res. Lett.* **26,** 2089–2092.

Ida, Y. (1972). Cohesive force across the tip of a longitudinal-shear crack and Griffith's specific surface energy, *J. Geophys. Res.* **77,** 3796–3805.

Ide, S., and M. Takeo (1997). Determination of constitutive relation of fault slip based on seismic wave analysis, *J. Geophys. Res.* **102,** 27,379–27,391.

Inoue, D., K. Miyakoshi, K. Ueta, and S. Abe (2001). Geological survey of active faults around the 2000 Tottori-Seibu earthquake, *Genshir-yoku-eye* [Nuclear Viewpoints] **47,** 66–71 (in Japanese).

Iwata, T., H. Sekiguchi, Y. Matsumoto, H. Miyake, and K. Irikura (2000). Source precess of the 2000 western Tottori prefecture earthquake and near-source strong ground motion, Presented at the 2000 Fall meeting of the Seismological Society of Japan, November 2000, Tsukuba, Japan.

Mikumo, T., and T. Miyatake (1995). Heterogeneous distribution of dynamic stress drop and relative fault strength recovered from the results of waveform inversion: the 1984 Morgan Hill, California, earthquake, *Bull. Seism. Soc. Am.* **85,** 178–193.

Mikumo, T., S. K. Singh, and M. A. Santoyo (1999). A possible stress interaction between large thrust and normal faulting earthquakes in the Mexican subduction zone, *Bull. Seism. Soc. Am.* **89,** 1418–1427.

Mikumo, T., K. B. Olsen, E. Fukuyama, and Y. Yagi (2003). Stress-breakdown time and slip-weakening distance inferred from slip-velocity functions on earthquakes faults, *Bull. Seism. Soc. Am.* **93,** 264–282.

Miyatake, T. (1992). Dynamic rupture process of inland earthquakes in Japan weak and strong asperity, *Geophys. Res. Lett.* **19,** 1041–1044.

Moore, D. E., and D. A. Lockner (1995). The role of microfracturing in shear-fracture propagation in granite, *J. Struct. Geol.* **17,** 95–114.

Nayfeh, A. H., and M. S. Hefsy (1978). Continuum modeling of three-dimensional truss-like space structures, *AIAA J.* **16,** 779–787.

Ohnaka, M., Y. Kuwahara, and K. Yamamoto (1987). Nucleation and propagation processes of stick-slip failure and normal stress dependence of the physical parameters of dynamic slip failure, *Nat. Disaster Sci.* **9,** 1–21.

Olsen, K. B., R. Madariaga, and R. Archuleta (1997). Three-dimensional dynamic simulation of the 1992 Landers earthquake, *Science* **278,** 834–838.

Petit, J. P., and M. Barquins (1988). Can natural faults propagate under mode II conditions? *Tectonics* **7,** 1243–1256.

Quin, H. (1990). Dynamic stress drop and rupture dynamic of the October 15, 1979 Imperial Valley, California, earthquake, *Tectonophysics* **175,** 93–117.

Riera, J. D., and M. Rocha (1991). A note on the velocity of crack propagation in tensile fracture, *Rev. Bras. Ciencias Mecanicas* **12,** no. 3, 217–240.

Sekiguchi, H., and T. Iwata (2001). Near-source ground motions controlled by source process in the case of the 2000 Tottori ken-Seibu earthquake, in Procedings of the 2001 SSJ Fall Meeting, October 2001, Kagoshima, Japan.

Shibutani, T., S. Nakao, R. Nishida, F. Takeuchi, K. Watanabe, and Y. Umeda (2002). Swarm-like seismic activity in 1989, 1990, and 1997 preceding the 2000 western Tottori earthquake, *Earth Planets Space* **54,** 831–845.

Ueta, K., K. Miyakoshi, and D. Inoue (2002). Left-lateral deformation of headrace tunnel associated with the 2000 western Tottori earthquake, *J. Seism. Soc. Japan* **54,** 547–556 (in Japanese with English abstract).

Vermilye, J. M., and C. H. Scholz (1998). The process zone: a microstructural view of fault growth, *J. Geophys. Res.* **103,** 12,223–12,237.

Yagi, Y. (2001). Source rupture process of the Tottori-ken Seibu earthquake of October 6, 2000 obtained by joint inversion of near-field and teleseismic data, Presented at the meeting of Japan Earth and Planetary Science, June 2001, Tokyo, Japan.

Disaster Prevention Research Institute
Kyoto University
Gokasho, Uji
Kyoto 611-0011, Japan
dalguer@egmdpri01.dpri.kyoto-u.ac.jp
irikura@egmdpri01.dpri.kyoto-u.ac.jp
(L.A.D., K.I.)

Curso de Pós Graduação de Engenharia Civil
Universidade Federal de Rio Grande do Sul
Av. Osvaldo Aranha 99, 3° andar, CEP 90035-190
Porto Alegre, R.S. Brazil
riera@genesis.cpgec.ufrgs.br
(J.D.R.)

Manuscript received 12 August 2002.